

LMA and sterile neutrinos: a case for resonance spin flavour precession?

Bhag C. Chauhan ^{*}and João Pulido

Centro de Física das Interacções Fundamentais (CFIF)

Departamento de Física, Instituto Superior Técnico

Av. Rovisco Pais, P-1049-001 Lisboa, Portugal

E-mail: chauhan@cfif.ist.utl.pt, pulido@cfif.ist.utl.pt

ABSTRACT: Open questions remain after the confirmation of LMA as the dominant solution to the solar neutrino deficit. These are the apparent time modulation of the solar neutrino event rates in the Homestake, Gallium and SuperKamiokande experiments, possibly related to solar magnetic activity, the discrepancy between the event rate in the Homestake experiment and its theoretical prediction and the absence of the electron spectrum upturn in SuperKamiokande at energies below 6-8 MeV. We search for a possible understanding of these questions in the context of resonant spin flavour precession to sterile neutrinos, assuming a class of magnetic field profiles anchored in the upper radiation/lower convection zone. We consider the simplest such model beyond the standard 2ν flavour LMA one, with one single magnetic moment transition between active and sterile state and vanishing vacuum mixing. The preferred mass square difference is $\Delta m_{10}^2 = O(10^{-8} \text{ eV}^2)$. The Ga rate appears to be the most sensitive of all to solar activity. It is also found that a field profile extending within a longer region in the radial direction is favoured over another with a shorter span, and leads to a stronger suppression than in the LMA case of the intermediate energy neutrinos and some of the 8B ones.

KEYWORDS: Solar Neutrinos, Sterile Neutrinos, LMA, Resonance Spin Flavour Precession.

THE P00 (2004) 000

^{*}On leave from Govt. Degree College, Karsog (H P) India 171304.

Contents

1. Introduction	1
2. Structure of the Model	2
3. Solutions and Discussion	6
4. Conclusions	11

1. Introduction

The KamLAND experiment [1] seems to confirm the Large Mixing Angle (LMA) solution to the solar neutrino deficit, originally presented in 1992 [2], and to rule out spin flavour precession (SFP) [3]. Even the possibility of a sub-dominant SFP is substantially constrained [4] in view of the recent upper bound on solar antineutrinos corresponding to 0.028% of the 8B neutrino flux obtained by the KamLAND collaboration [5]. It would be however premature to assert that LMA [6] is the final and complete solution, at a time when solar neutrino experiments enter a new era of precision measurements and there are hints of possible phenomena which fail to fit in this scenario.

One of the generic predictions of LMA is an exceedingly large rate [7] for the Cl experiment [8]. This discrepancy reaches an excess of 2.5σ if one uses the latest BP'04 results [9]. Moreover, despite accurate predictions for the SuperKamiokande [10] and SNO [11] total reduced rates, the corresponding LMA spectrum predictions exhibit an upturn below (6-8) MeV which is absent in both data. While the absolute values of the rates may not be significant, because they involve a normalization to a specific 8B flux whose value is known within a (15-20)% theoretical uncertainty, the absence of this upturn in the data may motivate new physics beyond LMA, since it does not rely on normalization to a specific model¹. Reconciling the theory with the data in this aspect implies a decrease in the survival probability for neutrinos with energies in the range (0.8-8) MeV, that is, those which are observed by Chlorine and unobserved by SK and SNO.

Another hint which may point to new physics lies in the possible time dependence of the neutrino signal. Solar neutrino statistical analyses confronting theoretical model predictions with data have been using time averaged event rates or fluxes [6, 12] and could, for this reason, be missing important information. The examination of the data on a time basis by the Stanford Group has in fact provided increasing evidence that the solar neutrino flux is not constant, but varies with well-known solar rotation periods [13, 14, 15]. Such a

¹The present statistics both in SK and SNO are however not enough to perform a strict statement concerning acceptance or rejection of a model only on grounds of this upturn.

situation, if confirmed, can in no way be explained by the LMA scenario. It can neither be understood in terms of an SFP transition of ν_e into $\bar{\nu}_\mu$ or $\bar{\nu}_\tau$ [4], as this would originate a sizable and unseen $\bar{\nu}_e$ flux.

The intermediate energy dip in the survival probability and the possibility of modulation of the neutrino signal constitute our main motivation to investigate scenarios with a sterile neutrino. A magnetic moment driven conversion from active to sterile neutrinos and the fact that these leave no trace in the detectors appears to be an attractive possibility to generate these two effects. In fact, time dependence requires this conversion to be related to solar magnetic activity or to solar rotation with an axially asymmetric magnetic field profile.

Our purpose in this paper is to perform a combined prediction of all solar neutrino data, namely the rates for Chlorine [8] and Gallium [16], [17] experiments, the SuperKamiokande [10] reduced rate and spectrum and the reduced rates in SNO data [11]. We will not be concerned at this preliminary stage with χ^2 fittings, but rather with showing the change in the LMA probability shape and solar neutrino predictions resulting from a possible time dependent magnetic field related conversion to the sterile neutrino. In section 2 we present the general structure of the model, in section 3 we derive the numerical predictions of all rates and discuss other consequences of the model for two specific solar field profiles and in section 4 we draw our main conclusions.

2. Structure of the Model

In order to expound our model, we consider a system of two active neutrinos and a sterile one which mix in the mass eigenstates ν_0 , ν_1 and ν_2 . This can be parametrized by the following rotation matrix [18]

$$\begin{pmatrix} \nu_s \\ \nu_e \\ \nu_x \end{pmatrix} = \begin{pmatrix} c_\alpha & s_\alpha & 0 \\ -s_\alpha c_\theta & c_\alpha c_\theta & s_\theta \\ s_\alpha s_\theta & -c_\alpha s_\theta & c_\theta \end{pmatrix} \begin{pmatrix} \nu_0 \\ \nu_1 \\ \nu_2 \end{pmatrix} \quad (2.1)$$

with θ denoting the usual LMA vacuum mixing angle and α the vacuum sterile mixing. A straightforward but tedious calculation then leads to the following form of the vacuum Hamiltonian

$$\mathcal{H}_{\text{vac}} = \begin{pmatrix} \frac{-\Delta m_{10}^2}{2E} c_\alpha^2 & \frac{\Delta m_{10}^2}{4E} s_{2\alpha} c_\theta & \frac{-\Delta m_{10}^2}{4E} s_{2\alpha} s_\theta \\ \frac{\Delta m_{10}^2}{4E} s_{2\alpha} c_\theta & \frac{\Delta m_{21}^2}{2E} s_\theta^2 - \frac{\Delta m_{10}^2}{2E} s_\alpha^2 c_\theta^2 & \left(\frac{\Delta m_{21}^2}{4E} + \frac{\Delta m_{10}^2}{4E} s_\alpha^2\right) s_{2\theta} \\ \frac{-\Delta m_{10}^2}{4E} s_{2\alpha} s_\theta & \left(\frac{\Delta m_{21}^2}{4E} + \frac{\Delta m_{10}^2}{4E} s_\alpha^2\right) s_{2\theta} & \frac{\Delta m_{21}^2}{2E} c_\theta^2 - \frac{\Delta m_{10}^2}{2E} s_\alpha^2 s_\theta^2 \end{pmatrix} \quad (2.2)$$

with obvious notation. We seek for a model which should be the simplest departure from the conventional LMA case and be able to generate a time dependent transition into a sterile neutrino. To this end we take a vanishing mixing angle, $\alpha=0$, so that active states ν_e , ν_μ communicate to the sterile one through magnetic moment transitions only. The

matter Hamiltonian is thus

$$\mathcal{H}_M = \begin{pmatrix} \frac{-\Delta m_{10}^2}{2E} & \mu_1 B & \mu_2 B \\ \mu_1 B & \frac{\Delta m_{21}^2}{2E} s_\theta^2 + V_e & \frac{\Delta m_{21}^2}{4E} s_{2\theta} \\ \mu_2 B & \frac{\Delta m_{21}^2}{4E} s_{2\theta} & \frac{\Delta m_{21}^2}{2E} c_\theta^2 + V_\mu \end{pmatrix} \quad (2.3)$$

with V_e and V_μ being the matter induced potentials for ν_e and ν_μ respectively and μ_1, μ_2 their transition moments to the sterile neutrino. We will consider field profiles concentrated around the bottom of the convective zone, as motivated by the dynamo theory [13, 14, 15], and hence require spin flavour precession to be resonant in this region. Therefore the two processes (LMA and RSFP) occur sequentially at very different solar radii, with the RSFP critical density determined by a mass square difference between one of the active states and the sterile one $O(10^{-8} eV^2)$. An efficient conversion to the sterile neutrino requires that the transition moment associated with this order of magnitude difference dominates over the other. Given these facts we choose $\Delta m_{10}^2 = O(10^{-8} eV^2)$ and so $\mu_2 = 0$. ²

We obtain the neutrino survival probability ($P(\nu_e \rightarrow \nu_e) = P_{ee}$) by assuming the propagation inside the sun to be adiabatic except in the region where the adiabaticity parameter reaches its minimum. This is essentially a generalization of the (2x2) case proposed some time ago [19]. In fig.1 we show the evolution of the mass matter eigenvalues inside the sun for a typical case. It corresponds to a neutrino energy $E = 2.1 MeV$, $\Delta m_{10}^2 = -1.7 \times 10^{-8} eV^2$ and field profile 2 described below with peak field $B_0 = 3.0 \times 10^5 G$. Of the three eigenvalues, it is seen that ν_1 and ν_0 become the closest in the convection zone ($r/R_S \simeq 0.8$), so that adiabaticity may be broken in the transition at this critical density. We recall that a strong field in this region will provide an efficient, adiabatic conversion corresponding to a larger eigenvalue separation while a weaker field will generate less conversion, with closer eigenvalues. Moreover the LMA oscillation and the $\nu_2 \rightarrow \nu_0$ transition are strongly adiabatic. This suggests that a field profile exhibiting a time dependent peak value deep inside the convective zone will manifest itself in the modulation of the neutrino signal. Hence we need only to consider the jump probability P_C between ν_1 and ν_0 and the expression describing the three neutrino propagation is

$$\begin{pmatrix} \nu_s(t) \\ \nu_e(t) \\ \nu_\mu(t) \end{pmatrix} = [R_o^T] [A] [B] [C] [R_i] \begin{pmatrix} 0 \\ 1 \\ 0 \end{pmatrix} \quad (2.4)$$

where

$$[A] = \begin{pmatrix} e^{-i \int_{r_x}^{r_o} H_{D11} dr} & & \\ & e^{-i \int_{r_x}^{r_o} H_{D22} dr} & \\ & & e^{-i \int_{r_x}^{r_o} H_{D33} dr} \end{pmatrix} \quad (2.5)$$

$$[B] = \begin{pmatrix} \sqrt{1 - P_C} & \sqrt{P_C} & 0 \\ \sqrt{P_C} & \sqrt{1 - P_C} & 0 \\ 0 & 0 & 1 \end{pmatrix} \quad (2.6)$$

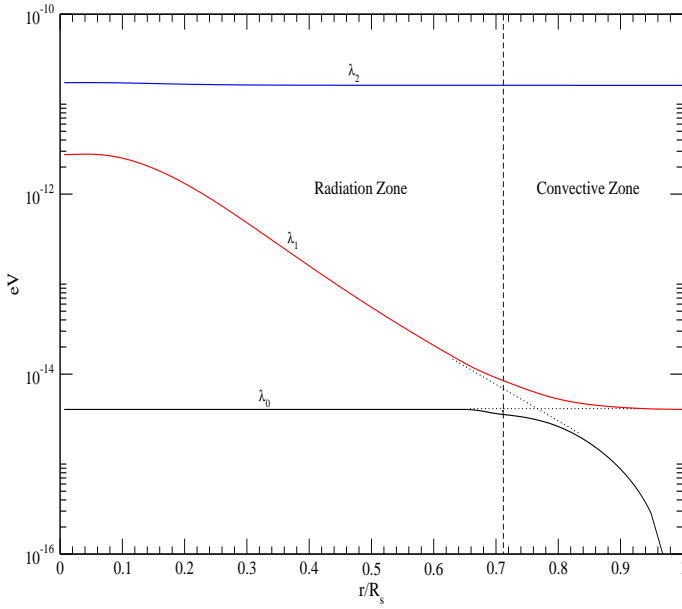


Figure 1: The evolution of the mass matter eigenvalues along the solar neutrino trajectory. The example chosen is for profile 2 (see fig.2) with neutrino energy $E = 2.1\text{MeV}$, $\Delta m_{10}^2 = -1.7 \times 10^{-8}\text{eV}^2$, $B_0 = 3.0 \times 10^5\text{G}$. LMA parameters are slightly shifted from their best fit values [11]: $\Delta m_{21}^2 = 6.8 \times 10^{-5}\text{eV}^2$, $\theta = 32.1^\circ$.

$$[C] = \begin{pmatrix} e^{-i \int_{r_i}^{r_x} H_{D11} dr} & & \\ & e^{-i \int_{r_i}^{r_x} H_{D22} dr} & \\ & & e^{-i \int_{r_i}^{r_x} H_{D33} dr} \end{pmatrix} \quad (2.7)$$

Here H_D denotes the diagonalized Hamiltonian, r_i the neutrino production point, r_o the detection point and r_x the location of the RSFP critical density. $[R]$ is the rotation matrix from the weak eigenstate to the matter eigenstate basis. Its form in the vacuum is given by the transpose of (2.1) with $\alpha = 0$. In matter with magnetic field it becomes in its most general form

$$[R] = \begin{pmatrix} c_{01}c_{02} & -s_{01}c_{12}-c_{01}s_{12}s_{02} & s_{01}s_{12}-c_{01}c_{12}s_{02} \\ s_{01}c_{02} & c_{01}c_{12}-s_{01}s_{12}s_{02} & -c_{01}s_{12}-s_{01}c_{12}s_{02} \\ s_{02} & s_{12}c_{02} & c_{12}c_{02} \end{pmatrix} \quad (2.8)$$

where θ_{01} , θ_{02} are the mixing angles induced by the neutrino magnetic moments μ_1 , μ_2 respectively. The matter mixing angle θ_{12} becomes in the vacuum the LMA mixing angle θ , eq. (2.1). In equation (2.4) $[R_i]$ converts the weak eigenstate ν_e produced in the solar core into a combination of Hamiltonian eigenstates which propagate adiabatically (matrices $[C]$ and $[A]$) except for the correction at the critical density described by the matrix $[B]$ where

²The other situation, namely a non-vanishing μ_2 and $\mu_1 = 0$ would correspond very closely to the LMA one and two sizable transition moments to an intermediate possibility.

ν_1 and ν_0 nearly meet. In order to account for level crossing at the resonance between states ν_0 , ν_1 , the corresponding first two rows of the rotation matrix R are interchanged so as to obtain R_o . Hamiltonian eigenstates are then converted back to the weak basis through R_o^T at the detection point. Taking $\theta_{02} = 0$ ($\mu_2 = 0$) and using eq.(2.8), matrices $[R_i]$ and $[R_o^T]$ therefore read

$$[R_i] = \begin{pmatrix} c_{01} & -s_{01}c_{12} & s_{01}s_{12} \\ s_{01} & c_{01}c_{12} & -c_{01}s_{12} \\ 0 & s_{12} & c_{12} \end{pmatrix} \quad (2.9)$$

$$[R_o^T] = \begin{pmatrix} s_{01} & c_{01} & 0 \\ c_{01}c_{12} & -s_{01}c_{12} & s_{12} \\ -c_{01}s_{12} & s_{01}s_{12} & c_{12} \end{pmatrix} \quad (2.10)$$

For the jump probability P_C we use the Landau Zener approximation

$$P_C = \exp\left(-\frac{\pi}{2}\gamma_C\right) \quad (2.11)$$

with the adiabaticity parameter given by the ratio between the corresponding eigenvalue difference and the spatial rate of the mixing angle

$$\gamma_C = \left| \frac{\lambda_0 - \lambda_1}{2\dot{\theta}_{01}} \right|. \quad (2.12)$$

Using equations (2.4) - (2.10) and the fact that at the neutrino production and detection points the absence of magnetic field implies the vanishing of angle θ_{01} , the expressions for the survival and conversion probabilities become

$$P_{ee} = |(\nu_e(t), \nu_e)|^2 = c_\theta^2 c_{12i}^2 P_C + s_\theta^2 s_{12i}^2 \quad (2.13)$$

$$P_{e\mu} = |(\nu_\mu(t), \nu_e)|^2 = s_\theta^2 c_{12i}^2 P_C + c_\theta^2 s_{12i}^2 \quad (2.14)$$

where we neglected fast oscillating terms which average to zero and subscript i refers to the mixing angle at the production point. The LMA survival and conversion probabilities in the 2-flavour case can be readily obtained from eqs. (2.13), (2.14) for $P_C = 1$ (vanishing magnetic field at the resonance point).

The expression for the SK spectrum to be used is

$$R_{SK}^{th} = \frac{\int_{E_{emin}}^{E_{emax}} dE_e \int_{m_e}^{E'_e} dE'_e f(E'_e, E_e) \int_{E_m}^{E_M} dE \phi(E) [P_{ee}(E) \frac{d\sigma_{\nu_e}}{dT'} + P_{e\mu}(E) \frac{d\sigma_{\nu_\mu}}{dT'}]}{\int_{E_{emin}}^{E_{emax}} dE_e \int_{m_e}^{E'_e} dE'_e f(E'_e, E_e) \int_{E_m}^{E_M} dE \phi(E) \frac{d\sigma_{\nu_e}}{dT'}} \quad (2.15)$$

with standard notation [20] and a similar expression for the SNO one. We take the SK and SNO energy resolution functions from [21],[22].

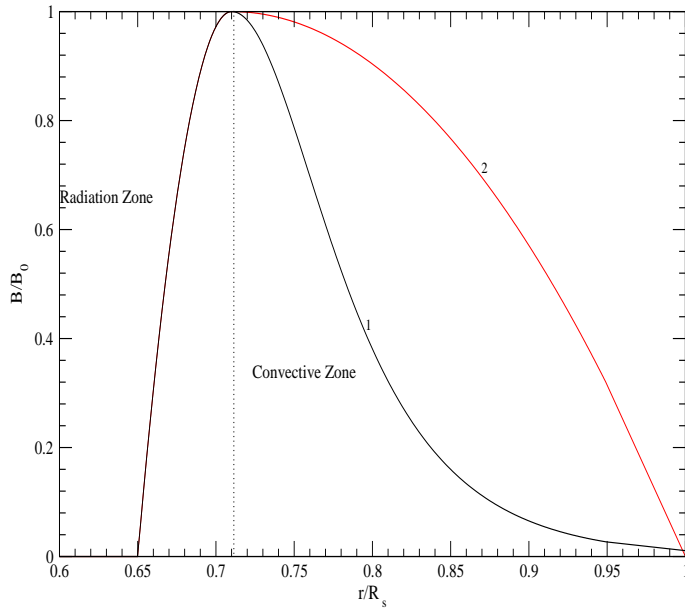


Figure 2: Solar magnetic field profiles. These are motivated by the dynamo process near the tachocline [15]: they exhibit a common and fast rise starting at the upper radiation zone reaching a peak at the bottom of the convection zone. Profile 2 extends over a longer region, hence it leads to more efficient sterile neutrino conversion.

3. Solutions and Discussion

The two classes of field profiles to be used are characterized by a sharp increase starting in the radiative zone just below the tachocline, reaching a peak at the bottom of the convective zone and a smoother decrease up to the solar surface. They are (see fig.2)

Profile 1

$$B = B_0 \left(1 - \left(\frac{x - x_C}{0.06} \right)^2 \right) , \quad x_R \leq x \leq x_C \quad (3.1)$$

$$B = \frac{B_0}{\cosh(18(x - x_C))} , \quad x_C < x \leq 1 \quad (3.2)$$

Profile 2

$$B = B_0 \left(1 - \left(\frac{x - x_C}{0.06} \right)^2 \right) , \quad x_R \leq x \leq x_C \quad (3.3)$$

$$B = B_0 \left(1 - \left(\frac{x - x_C}{1 - x_C} \right)^2 \right) , \quad x_C < x \leq 1 \quad (3.4)$$

with vanishing field for $x < x_R$. Here x is the fraction of the solar radius, $x_R = 0.65$, $x_C = 0.71$ and we take in all cases a magnetic moment $\mu_1 = 10^{-12} \mu_B$. The preferred peak field values are found to be in the range $B_0 = (2 - 3) \times 10^5 G$.

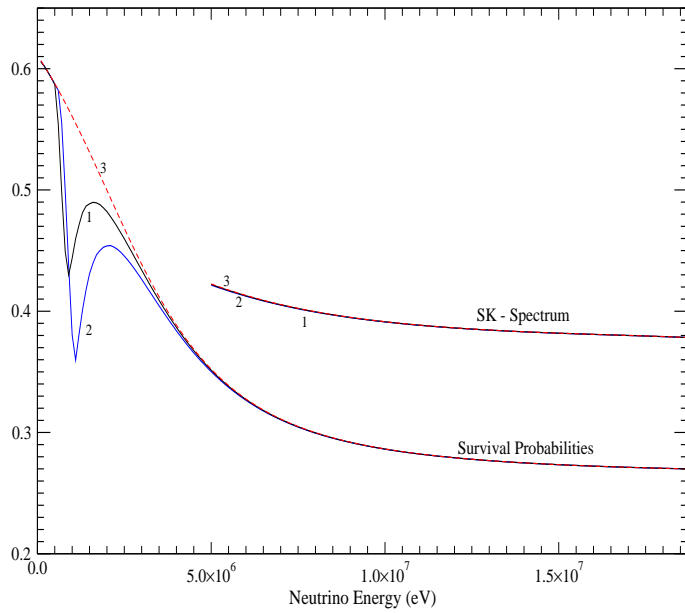


Figure 3: Survival probabilities and SuperKamiokande spectrum for profile 1 (curves 1 and 2). For comparison, the LMA curves are also given (curves 3). The dip in the probability hardly affects the shape of the spectrum. (See also table II).

In table I we show the solar neutrino data on rates and their comparison with the SSM [9] predictions including the theoretical uncertainties ³. We refer to the parameter values as given from global fits [11] $\Delta m_{21}^2 = 7.1 \pm 1.2 \times 10^{-6} \text{ eV}^2$, $\theta = 32.5 \pm 2.4$ degrees. Our main results are summarized in figs.3 - 6 and tables II, III.

Experiment	Data	Theory	Data/Theory	Reference
Homestake	$2.56 \pm 0.16 \pm 0.15$	8.5 ± 1.8	0.301 ± 0.069	[8]
SAGE	$70.9 \pm 5.3 \pm 3.7$	131 ± 12	0.541 ± 0.070	[17]
Gallex+GNO	$70.8 \pm 4.5 \pm 3.8$	131 ± 12	0.540 ± 0.067	[16]
SuperKamiokande	$2.35 \pm 0.02 \pm 0.08$	5.82 ± 1.34	0.404 ± 0.094	[10]
SNO CC	$1.59 \pm 0.08 \pm 0.06$	5.82 ± 1.34	0.273 ± 0.065	[11]
SNO ES	$2.21 \pm 0.31 \pm 0.10$	5.82 ± 1.34	0.380 ± 0.104	[11]
SNO NC	$5.21 \pm 0.27 \pm 0.38$	5.82 ± 1.34	0.895 ± 0.221	[11]

Table I - Data from the solar neutrino experiments. Units are SNU for Homestake and Gallium and $10^6 \text{ cm}^{-2} \text{ s}^{-1}$ for SuperKamiokande and SNO. The uncertainties in the fourth column include solar standard model errors.

³Here we use the BP04 standard solar model [9].

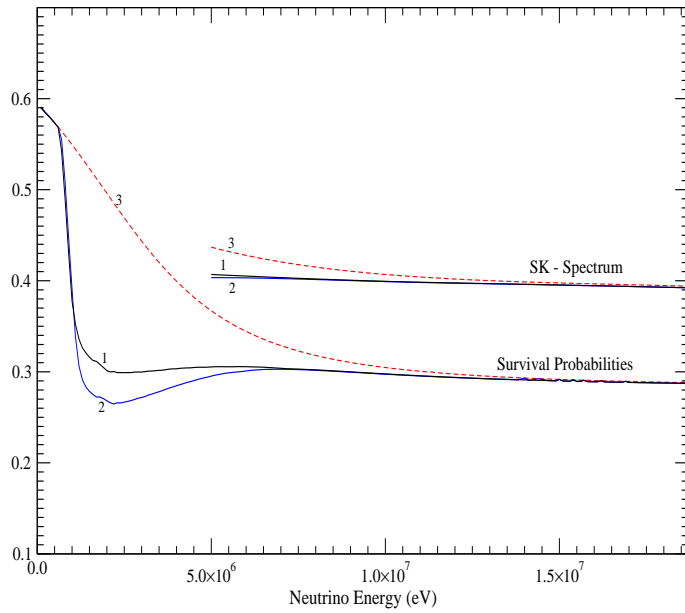


Figure 4: Same as fig.3 for profile 2. A downturn of the spectrum appears in this case as some 8B neutrinos ($E > 5\text{MeV}$) are converted to sterile ones. (See also table III).

$\Delta m_{10}^2 (\text{eV}^2)$	$B_0(\text{G})$	Cl	Ga	SK	SNO_{CC}	SNO_{ES}	SNO_{NC}
$-1.35 \times 10^{-8}\text{eV}^2$	$2.0 \times 10^5\text{G}$	2.77	66.5	0.406	0.284	0.481	0.999
$-1.65 \times 10^{-8}\text{eV}^2$	$2.6 \times 10^5\text{G}$	2.76	66.9	0.406	0.284	0.476	0.999

Table II - Profile 1: Model predictions for rates. Units are SNU for Cl, Ga and the ratio of the model prediction by the SSM value for SK and SNO. See also fig.3 for the survival probabilities and SK spectrum. Here $\Delta m_{21}^2 (\text{eV}^2) = 6.5 \times 10^{-5}\text{eV}^2$, $\theta = 30.9^\circ$.

Fig.3 (profile 1) and fig.4 (profile 2) show the electron neutrino survival probability and the electron energy spectrum in SK for two values of Δm_{10}^2 in each profile together with the LMA probability and spectrum, for comparison, near the pure LMA best fit point. It is seen that the upturn in the LMA spectrum can be reduced or made to disappear. A flat spectrum, as suggested by the data [10], is in fact obtained for a convenient choice of Δm_{10}^2 and B_0 in the case of profile 2 but not for profile 1. For both profiles, however, the Cl rate is substantially decreased from its LMA prediction of approximately 3.1 SNU (see tables II, III). Parameter Δm_{10}^2 also determines the location of the important $\nu_1 \rightarrow \nu_0$ resonance, with less negative values corresponding to resonances closer to the solar surface. Also the longer spatial extension of a strong field in the case of profile 2 implies more conversion efficiency, a fact which is clearly reflected in a wider dip in the probability curve and even a flatness in the spectrum for $\Delta m_{10}^2 = -(1.6 - 1.7) \times 10^{-8} \text{ eV}^2$. All rates can be brought to within 1σ of the experimental value with theoretical errors included. In view of our motivation to account for possible modulations in the rates, we will not attempt at

quantitative and detailed fits at this stage, since the solar neutrino data used are averages and further, they do not refer to the same periods in different experiments.

Δm_{10}^2 (eV 2)	B_0 (G)	Cl	Ga	SK	SNO_{CC}	SNO_{ES}	SNO_{NC}
-1.6×10^{-8} eV 2	2.6×10^5	2.76	65.1	0.403	0.297	0.431	0.982
-1.7×10^{-8} eV 2	3×10^5	2.76	65.5	0.402	0.297	0.421	0.981

Table III - Same as table II for profile 2. See also fig.4 for the survival probabilities and SK spectrum. Here Δm_{21}^2 (eV 2) = 6.8×10^{-5} eV 2 , $\theta = 32.1^\circ$.

We note that the predictions from profiles 1 and 2 exhibit a manifest difference: in fact for profile 2 increasing the dip in the probability through an increase in the peak field leads to a stronger downturn of the spectrum, while for profile 1 an increase in the peak field leaves the spectrum unaffected (figs.3 and 4). This is because in profile 2 a higher peak field leads to a stronger suppression of the low energy sector of the 8B neutrinos, which are present in the SK rate, along with pep and CNO ones. For profile 1, which is more localized, an increase in the peak field affects only the suppression of the intermediate energy neutrinos in Cl, especially the pep neutrinos with energy $E_{pep} = 1.44$ MeV and the CNO ones, all absent in the SK rate and accounting for only a minor fraction of the Cl rate.

In figs.5, 6 we show the dependence of rates on the peak field value for profiles 1, 2, from a starting point with unaffected LMA predictions, up to $B_0 = 3 \times 10^5$ G [23] with a view on a possible anticipation of future studies of time dependence in neutrino signals. Four different cases of Δm_{10}^2 in the relevant range (10 $^{-8}$ eV 2) are considered (see table IV). The values of Δm_{21}^2 and θ are slightly different in figs.5 and 6, hence the small discrepancy in the rates in the pure LMA limit. They are however well within their 1σ range [11] (see the captions of tables II, III). We find that the Ga rate is the most sensitive of all to changes in B_0 with a maximum modulation for profiles 1 and 2 respectively

$$\frac{\Delta R_{Ga}}{R_{Ga}} \simeq 22\% , \quad \frac{\Delta R_{Ga}}{R_{Ga}} \simeq 40\% \quad (3.5)$$

At this point it should be noted that in their detailed analysis, the Stanford Group [13] finds the Ga rate to exhibit the most manifest time dependence of all with two clear peaks in the ranges 45-75 and 90-120 SNU. It is unclear at this stage whether this apparent convergence of results is essential or not, a situation which obviously deserves further investigation.

	a	b	c	d
Profile 1	-0.5×10^{-8} eV 2	-1.35×10^{-8} eV 2	-1.65×10^{-8} eV 2	-5×10^{-8} eV 2
Profile 2	-0.5×10^{-8} eV 2	-1.6×10^{-8} eV 2	-1.7×10^{-8} eV 2	-5×10^{-8} eV 2

Table IV - The values of Δm_{10}^2 labeled a, b, c, d in figures 5 and 6.

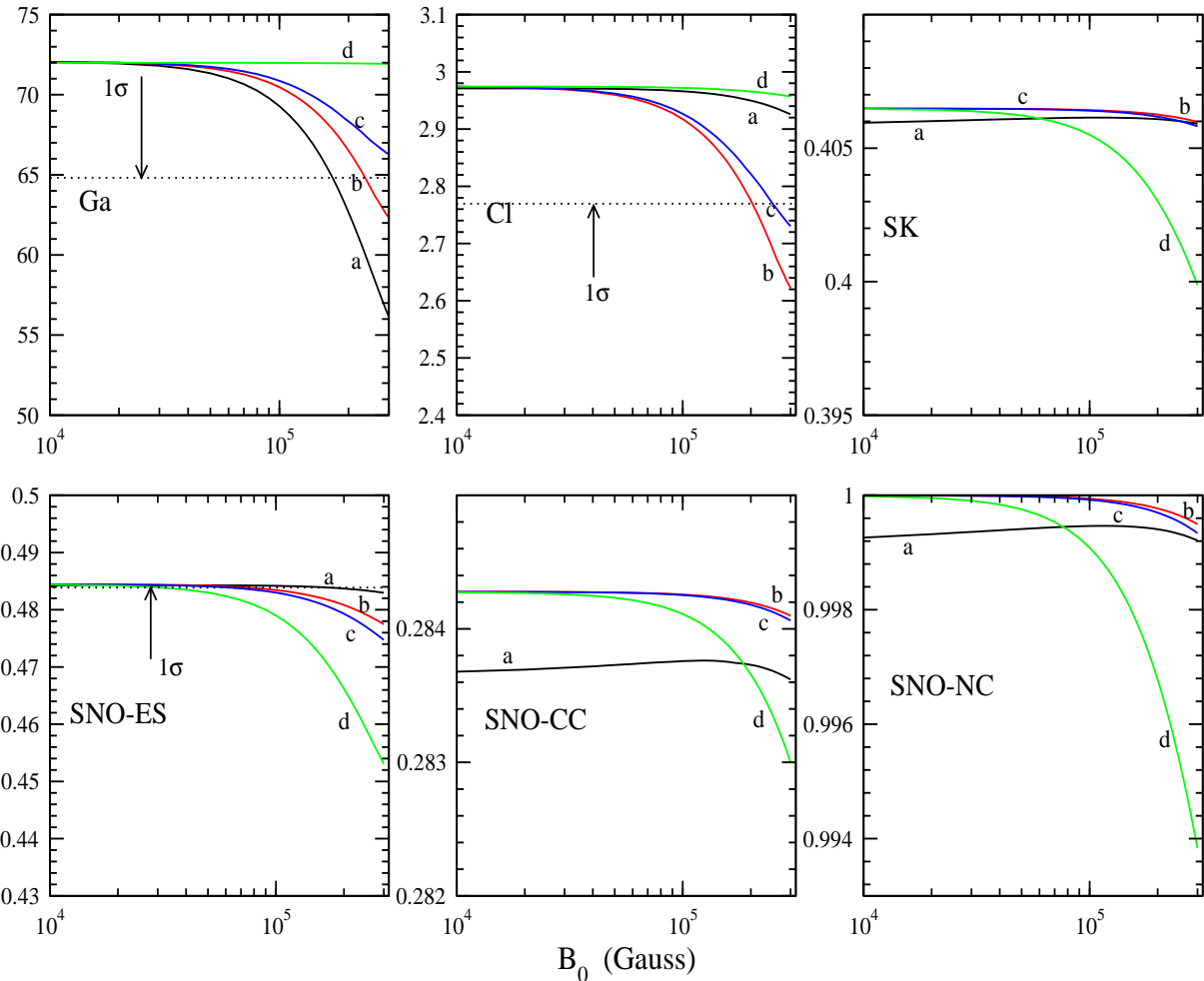


Figure 5: Event rates as a function of the peak field B_0 for profile 1. Variations of solar activity, manifested in a variable field intensity, are reflected in variations of the event rates. SK, SNO-CC and SNO-NC panels are all within 1σ of the experimental value including theoretical errors. The LMA parameters are slightly shifted from their best fit values [11]. (See also table IV).

The Cl rate is less sensitive with a maximum

$$\frac{\Delta R_{Cl}}{R_{Cl}} \simeq 12\% , \quad \frac{\Delta R_{Cl}}{R_{Cl}} \simeq 17\% \quad (3.6)$$

for profile 1 and profile 2 respectively. For all other rates this sensitivity is always below 7% for profile 1 and 15% for profile 2. All these modulations depend of course on the value of Δm_{10}^2 chosen. Furthermore the relative sensitivities of different rates to Δm_{10}^2 change from one rate to another. The cases described in detail in tables II, III and figs. 3, 4 can also be seen in a different context in figs. 5, 6.

In all our calculations we have used a neutrino magnetic moment $\mu_\nu = 10^{-12} \mu_B$. This is larger than the supernova bound [24, 25] by an approximate factor of 2 which applies for active-sterile magnetic moment conversions. Hence, if strictly enforced, this bound

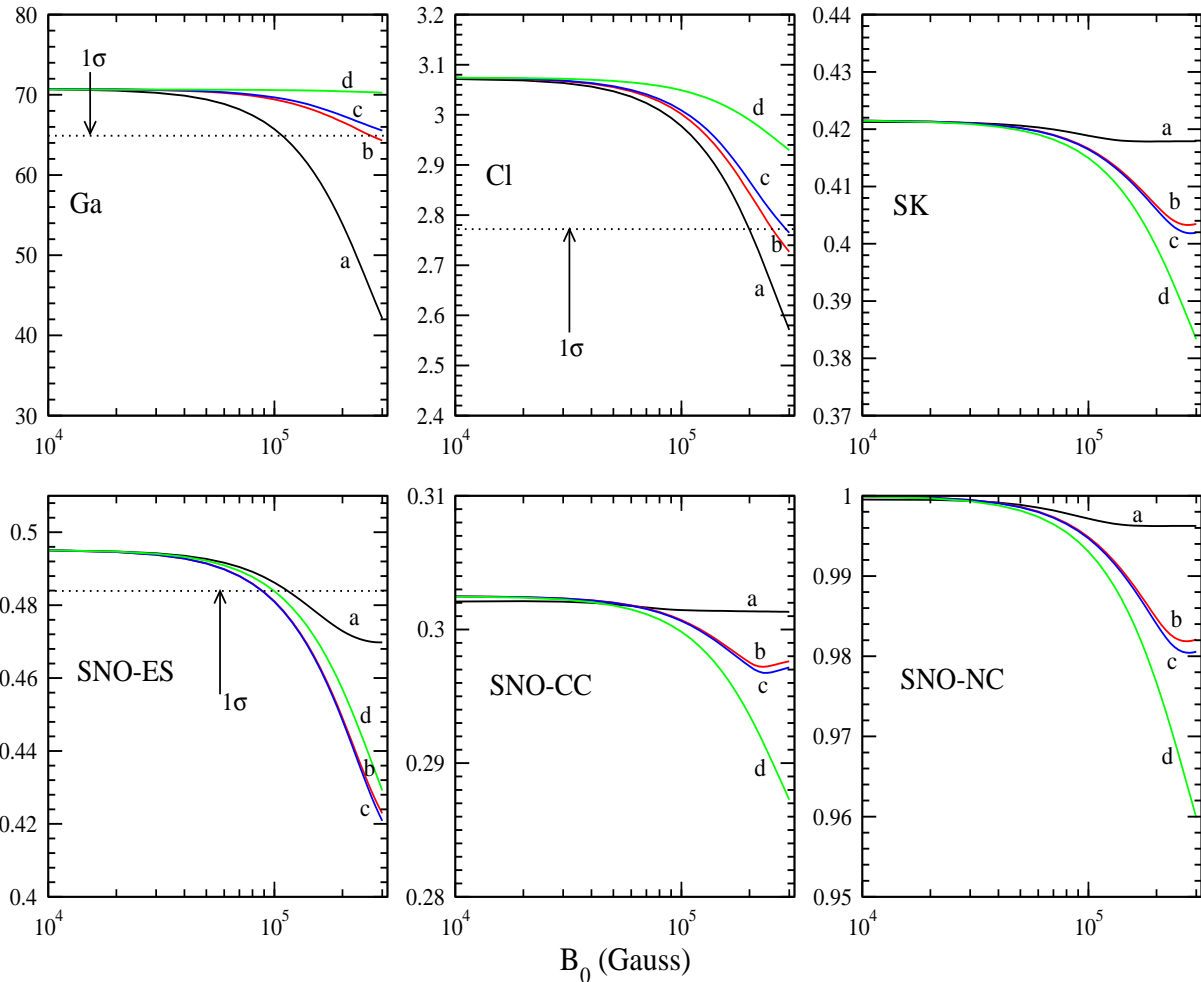


Figure 6: Same as fig.5 for profile 2. The LMA parameters are slightly shifted from their best fit values [11]. (See also table IV).

would require a peak field value of $(4 - 6) \times 10^5 G$ instead of $(2 - 3) \times 10^5 G$. However the supernova bound is plagued by uncertainties in the models of the supernova core [25] or based on rough estimates of the supernova energetic [24], so it cannot be expected to be quite stringent. On the other hand the solar magnetic field profile is poorly known, both in shape and strength. Whereas a field of the order of $3 \times 10^5 G$ is quite possible in the tachocline [23], it is not clear whether this can be exceeded by an extra factor of (1.5-2) or whether this factor could come from intrinsic inaccuracy of the supernova bound.

4. Conclusions

To conclude, now that KamLAND has established that LMA is the dominant solution to the solar neutrino problem, there remain a few questions, which may turn out to be quite important, as LMA may be incomplete and new physics might be necessary. To this end, the hints from solar neutrinos are a possible time variation of the neutrino event rate

[13, 14, 15] in the experiments, the absence of an electron spectrum upturn for low energies in opposition to the LMA expectation, and a rate in the Cl experiment lower than the LMA predicted one.

We proposed an answer to these questions by adding a sterile state to the two solar neutrino system. Such scenarios have already been developed in the literature [18, 26] in the context of oscillations alone, in particular it was shown that a sterile state may provide a solution to the above questions [18], except for the possible time modulation. Visible states communicate in those models with the sterile one via a vacuum mixing angle. In the model proposed in this paper, they communicate instead with the sterile one via magnetic moment transitions, so that time dependence of neutrino signals, if confirmed, can be directly connected to solar magnetic activity or to solar rotation. The new mass square difference is about three orders of magnitude below the LMA one, so that the transition to the sterile state resonates mainly in the tachocline, where the solar magnetic field is expected to be concentrated. In this way, a situation in which the transition moment associated with the smallest mass square difference dominates over the other leads to the most efficient conversion.

The upturn in the spectrum can remain unchanged, be reduced or eliminated, depending on the choice of this mass square difference and the field profile. As far as the Cl rate prediction is concerned, a sizable reduction from its LMA value is always obtained in the class of field profiles investigated. Profiles 1 and 2 illustrate these situations: the elimination of the spectrum upturn may or may not accompany the reduction in the Cl rate (profiles 2 and 1 respectively). It should be noted however that both SK and SNO data do not contain at present enough statistics that allow a strict statement on the exact spectrum shape.

We have also investigated the evolution of the event rates with the peak field values in each of the two profiles and found the Ga one to be the most sensitive of all. Interestingly enough, it was found by the Stanford Group [13] from a combined analysis of Gallex-GNO and SAGE that the Ga rate exhibits a strong time dependence with two clear peaks at 45-75 and 90-120 SNU. This apparent convergence between ours and their results certainly deserves further investigation. The Cl rate comes next to the Ga one in sensitivity, followed by all others (see figs.5, 6). In all cases we used the convenient mass square difference order of magnitude, $\Delta m_{10}^2 = O(10^{-8} eV^2)$. Profile 2, with a longer spatial extension, leads to more sensitivity of the rates. We have not performed χ^2 fittings, as, within the motivation of the present paper, they will be justified only for time dependent solar neutrino data which may soon become available.

Finally, the uncertainties both in the supernova neutrino magnetic moment bound and in the solar field profile make it premature to discard or rule out the present analysis.

Acknowledgements

We acknowledge useful discussions with Peter Sturrock and David Caldwell. The work of BCC was supported by Funda o para a Ci ncia e a Tecnologia through the grant SFRH/BPD/5719/2001.

References

- [1] [KamLAND Collaboration], K. Eguchi *et al.* Phys. Rev. Lett. **90**, 021802 (2003), arXiv:hep-ex/0212021.
- [2] [Gallex Collaboration], D. Vignaud in: J. R. Sanford, Proc. of XXVI Int. Conf. on High Energy Physics, Dallas, Texas, 1992, p.1093, AIP Conf. Proc. 272.
- [3] J.Schechter and J.W.F.Valle, Phys. Rev. **D24** 1883 (1981); C.S. Lim and W.J. Marciano, Phys. Rev. **D37** 1368 (1988); E.Kh. Akhmedov, Yad. Fiz. **48** 599 (1988) [Sov. J. Nucl.Phys. **48** 382 (1988)]; Phys. Lett. **B 213** 64 (1988).
- [4] Bhag C. Chauhan, João Pulido and E. Torrente-Lujan, Phys. Rev **D68** 033015 (2003), arXiv:hep-ph/0304297; O.G. Miranda, T.I. Rashba, A.I. Rez, J.W.F. Valle, arXiv:hep-ph/0311014; E. Torrente-Lujan, JHEP **0304** 054 (2003), arXiv:hep-ph/0302082; E. Torrente-Lujan, Phys. Lett. **B 441**, 305 (1998) arXiv: hep-ph/9807426; P. Aliani, V. Antonelli, M. Picariello and E. Torrente-Lujan, JHEP **0302** 025 (2003), arXiv:hep-ph/0208089.
- [5] [KamLAND Collaboration], K.Eguchi *et al.* Phys. Rev. Lett. **92**, 071301 (2004), arXiv:hep-ex/0310047.
- [6] A.B. Balantekin, H. Yuksel, Phys.Rev. **D68** 113002 (2003), arXiv:hep-ph/0309079; M. Maltoni, T. Schwetz, M.A. Tortola, J.W.F. Valle, Phys.Rev. **D68** 113010 (2003), arXiv:hep-ph/0309130; A. Bandyopadhyay, S. Choubey, S. Goswami, S.T. Petcov, D.P. Roy , Phys. Lett. **B 583** 134 (2004), arXiv:hep-ph/0309174; P. Aliani, V. Antonelli, M. Picariello, E. Torrente-Lujan, Phys.Rev. **D69** 013005 (2004), arXiv:hep-ph/0212212; P.C.de Holanda and A.Yu. Smirnov, arXiv:hep-ph/0309299; J.N. Bahcall, M.C. Gonzalez-Garcia, C. Peña-Garay, JHEP **0302** 009 (2003).
- [7] P.C. de Holanda, A.Yu. Smirnov, Phys.Rev. **D66** 113005 (2002); Phys.Rev. **D66** 113005 (2002), arXiv:hep-ph/0205241.
- [8] [Homestake Collaboration], B.T. Cleveland, Astrophys. J. **496** 505 (1998).
- [9] J.N. Bahcall and M.H. Pinsonneault, Phys. Rev. Lett. **92**, 121301 (2004), astro-ph/0402114.
- [10] [SuperKamiokande Collaboration], S. Fukuda *et al.* Phys. Rev. Lett. **86** 5651 (2001), arXiv:hep-ex/0103032.
- [11] [SNO Collaboration], S.N.Ahmed *et al.*, Phys. Rev. Lett. **92**, 181301 (2004), arXiv:nucl-ex/0309004.
- [12] Bhag C. Chauhan and J. Pulido, Phys. Rev. **D66** 053006 (2002), arXiv:hep-ph/0206193.
- [13] P.A. Sturrock and J. Scargle, Astrophys. J. **550** L101 (2001).
- [14] P.A. Sturrock and M. Weber, Astrophys. J. **565** 1366 (2002).
- [15] D.O. Caldwell and P.A. Sturrock, arXiv:hep-ph/0309191.
- [16] [Gallex Collaboration], T.A. Kirsten, Nucl. Phys. B (Proc. Suppl.) **118** 33 (2003).
- [17] [SAGE Collaboration], V.N. Gavrin, Nucl. Phys. B (Proc. Suppl.) **118** 39 (2003).
- [18] P.C.de Holanda and A.Yu. Smirnov, arXiv:hep-ph/0307266.

- [19] S.J. Parke, Phys. Rev. Lett. **57** 1275 (1986); W.C. Haxton, Phys. Rev. Lett. **57** 1271 (1986); A. Dar *et al.*, Phys. Rev. **D35** 3607 (1987); S. Toshev, Mod. Phys. Lett. **A 3** 71 (1988); S. Toshev, Phys. Lett. **B 198** 551 (1988).
- [20] João Pulido, Astropart. Phys. **18** 173 (2002), arXiv:hep-ph/0112104.
- [21] [SuperKamiokande Collaboration], Y. Fukuda *et al.* Phys. Rev. Lett. **81** 1158 (1998), arXiv:hep-ex/9805021 .
- [22] [SNO homepage], <http://sno.phy.queensu.ca>.
- [23] H.M. Antia, S.M. Chitre and M.J. Thompson, Astron. Astrophys. **360** 335 (2000).
- [24] J. Lattimer and J. Cooperstein, Phys. Rev. Lett. **61** 23 (1988).
- [25] R. Barbieri and R. Mohapatra, Phys. Rev. Lett. **61** . 27 (1988).
- [26] V. Berezinsky, M. Narayan and F. Vissani, Nucl. Phys. **B658** 254 (2003), arXiv:hep-ph/0210204 ; P.C.de Holanda and A.Yu. Smirnov, arXiv:hep-ph/0211264.